Available online at www.sciencedirect.com
ScienceDirect
International Journal of Thermal Sciences 46 (2007) 1076–1083
International Journal of Thermal Sciences
www.elsevier.com/locate/ijts

Heat flux and slip effects on liquid flow in a microchannel

Guyh Dituba Ngoma *, Fouad Erchiqui

University of Quebec in Abitibi-Témiscamingue, Department of Applied Sciences, 445, Boulevard de l'Université, Rouyn-Noranda, Quebec, J9X 5E4, Canada

Received 3 July 2006; received in revised form 1 February 2007; accepted 2 February 2007

Available online 27 March 2007

Abstract

In this study, the liquid flow with the slip boundary condition in a microchannel between two parallel plates with imposed heat flux was numerically investigated. The combined effect of pressure-driven flow and electro-osmosis was taken into account. Electric potential, liquid flow and thermal characteristics were determined using the Poisson–Boltzmann, the modified Navier–Stokes and the energy equations for a hydrodynamical and thermal steady fully developed laminar flow for an incompressible liquid. The results demonstrate the influence of the slip coefficient, the heat flux and the pressure difference on flow velocity, local temperature and Nusselt number. A comparison of the developed model results with those in a previous study was made.
© 2007 Elsevier Masson SAS. All rights reserved.

Keywords: Microfluidics; Heat transfer; Microchannel; Slip flow; Modeling and simulation

1. Introduction

Developments in microfabrication technologies have led to the increased use of microfluidic transport in the fields of micropower generation, chemical processes, biomechanical processes, etc., where surface effects dominate the flow behavior within microdevices. An electric double layer (EDL) formed in a microchannel and containing an excess of counterions over co-ions to neutralize the surface charge plays a key role in the electro-osmotic flow. Its thickness is dependent on the bulk ionic concentration and electric fluid properties in a microchannel. Electro-osmotic pumps are suitable for fluid moving through microdevices because of the absence of moving parts and pulsating flows [1,2]. The surface chemical properties of a microchannel are extremely important in the movement and control of fluids at the microscopic level. In practice, hydrophobic surfaces are extensively used in microchannels for liquid flow. Thus, liquid flow modelling on the micro-scale will depend on the interactions between the fluid and the surface properties of the wall. Therefore, for efficient control and to ensure the reliability and the stability of the microfluidic devices with hydrophobic surfaces, detailed precise knowledge of the liquid flow behavior in microchannels, taking into account a correct boundary condition at the liquid–solid interface, is required [2,3]. Its investigation has to be considered in the planning and design phases of microfluidic devices. This makes it possible to avoid critical operating conditions. Most previous investigations of the pressure gradient and electro-osmotic liquid flow in microchannels were performed using a no-slip condition [4–12], whereas for the gas flow in microchannels, the slip boundary condition is accounted for [13–16]. Some previous experimental investigations have demonstrated the existence of liquid slip velocity on a microchannel, as reported in [3]. In addition, some previous studies were numerically performed considering a slip velocity for a liquid flow in a microchannel made from hydrophobic surfaces, taking into account an imposed electric field and a pressure gradient [16] without heat transfer considerations. Moreover, analysis of previous works shows that the results are specific to the microchannel configuration. Therefore, they cannot be extrapolated to other configurations. In the present work, the effects of slip coefficient and heat flux on a pressure-driven and electro-osmotic liquid flow in a microchannel between two plates are numerically investigated. The Poisson–Boltzmann, the modified Navier–Stokes and the energy equations are used to obtain a system of differential equations, which is solved to determine the distribution of flow velocity, volumetric flow

* Corresponding author.
E-mail address: guyh.dituba-ngoma@uqat.ca (G.D. Ngoma).

1290-0729/$ – see front matter © 2007 Elsevier Masson SAS. All rights reserved.
doi:10.1016/j.ijthermalsci.2007.02.001

Nomenclature

c_p	specific heat	$\mathrm{J\,kg^{-1}\,K^{-1}}$
e	elementary charge	C
E_x	external electric field strength	$\mathrm{V\,m^{-1}}$
h	distance between the plates	m
K	electrokinetic separation distance based on the distance between the plates	
K_{esd}	electrokinetic separation distance based on the half distance between the plates	
k	thermal conductivity	$\mathrm{W\,m^{-1}\,K^{-1}}$
k_b	Boltzmann constant	$\mathrm{J\,K^{-1}}$
L	plate length	m
n_∞	ionic number concentration in the bulk solution	$\mathrm{m^{-3}}$
Nu	Nusselt number	
p	pressure	Pa
Q	volumetric flow rate	$\mathrm{m\,s^{-3}}$
q	heat flux	$\mathrm{W\,m^{-2}}$
T	temperature	K
T_0	ambient temperature	K
u	flow velocity	$\mathrm{m\,s^{-1}}$
u_m	cross-sectional mean velocity	$\mathrm{m\,s^{-1}}$
u_0	reference velocity	$\mathrm{m\,s^{-1}}$
x	horizontal coordinate	m
y	vertical coordinate	m
z_0	valence of ions	

Greek

β	slip coefficient	m
Δ	difference	
ε	dimensionless dielectric constant	
ε_0	permittivity of vacuum	$\mathrm{C\,m^{-1}\,V^{-1}}$
ϕ	electric potential	V
γ	heat flux ratio	
κ	Debye–Hückle parameter	$\mathrm{m^{-1}}$
μ	viscosity	Pa s
ρ	fluid density	$\mathrm{kg\,m^{-3}}$
ρ_e	electric charge density	$\mathrm{C\,m^{-3}}$
σ	electric conductivity	$\Omega^{-1}\,\mathrm{m^{-1}}$
ζ	zeta potential	V

Subscripts

1	bottom plate wall
2	upper plate wall
m	mean value
w	wall

Superscripts

*	dimensionless parameter

rate, electric potential, temperature and mean Nusselt number. The boundary conditions for the slip velocity, the wall zeta potentials and the wall heat fluxes are accounted for in the final equations. Based on the equations found, a computer program was developed to analyze the effects of the pressure difference, the slip coefficient, the heat flux and the electrokinetic separation distance on the flow and thermal behavior of a liquid flow in a microchannel.

2. Mathematical formulation

Fig. 1 shows the examined model of the liquid flow in a microchannel between two parallel plates, which are separated by a distance h. The forced heat fluxes at the bottom and upper wall are q_1 and q_2, respectively. The zeta potentials at the bottom and upper wall are ζ_1 and ζ_2, respectively.

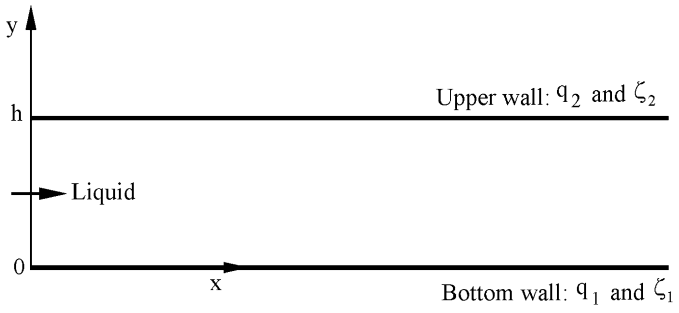

Fig. 1. Slip-flow in microchannel between the two parallel plates.

The following assumptions were made for the mathematical formulation:

(i) A steady state, one-dimensional and laminar flow was assumed.
(ii) Slip boundary conditions were assumed.
(iii) The slip coefficient was constant and the same at each microchannel wall.
(iv) A wall temperature jump was not considered.
(v) The wall heat flux was assumed to be constant.
(vi) The liquid was assumed to be incompressible.
(vii) A Newtonian liquid was assumed.
(viii) The liquid thermophysical properties were assumed to be constant.
(ix) A symmetric electrolyte was assumed.
(x) The electrical potential was assumed to be small compared to the thermal energy of the ions (Debye–Hückel approximation).

To account for these assumptions, the theoretical analysis of the liquid flow in a microchannel, as shown in Fig. 1, is based on the Poisson–Boltzmann, the modified Navier–Stokes and the energy equations.

2.1. Electric potential field

According to electrokinetics [1,2], the differential equation for the electric potential of ions, ϕ, in y-direction is given as

$$\frac{\mathrm{d}^2\phi}{\mathrm{d}y^2} = -\frac{\rho_e}{\varepsilon\varepsilon_0} \tag{1}$$

where ε represents the dielectric constant of the solution, ε_0 the permittivity of vacuum, and ρ_e the net charge density.

The net charge density, which is required to determine the electrostatic force caused by the presence of an EDL, can be written assuming a symmetric electrolyte as follows:

$$\rho_e = -2n_\infty z_0 e \sinh\left(\frac{z_0 e}{k_b T_0}\phi\right) \tag{2}$$

where e, k_b, n_∞, T_0 and z_0 are the elementary charge, Boltzmann constant, bulk concentration of ions, ambient temperature and valence of ions, respectively.

The other symbols, subscripts and superscripts used were defined in the nomenclature.

Substituting Eq. (2) into Eq. (1) yields

$$\frac{\mathrm{d}^2\phi}{\mathrm{d}y^2} = \frac{2n_\infty z_0 e}{\varepsilon\varepsilon_0}\sinh\left(\frac{z_0 e}{k_b T_0}\phi\right) \tag{3}$$

When using the Debye–Hückel approximation,

$$\frac{2n_\infty z_0 e}{\varepsilon\varepsilon_0}\sinh\left(\frac{z_0 e}{k_b T}\phi\right) \approx \frac{2n_\infty z_0 e}{\varepsilon\varepsilon_0}\frac{z_0 e}{k_b T}\phi \tag{4}$$

which physically means a small electric potential, in comparison with the thermal energy of ions, $|z_0 e\phi| < k_b T\,(|\phi| < 25\ \mathrm{mV}$ at 25 °C), Eq. (3) can be written as

$$\frac{\mathrm{d}^2\phi}{\mathrm{d}y^2} = \kappa^2\phi \tag{5}$$

where $\kappa = z_0 e\sqrt{\frac{2n_\infty}{\varepsilon\varepsilon_0 k_b T}}$ is the Debye–Hückel parameter and $1/\kappa$ is the Debye length.

Accounting for the Debye–Hückel approximation in Eq. (2) yields

$$\rho_e = -\varepsilon\varepsilon_0\kappa^2\phi \tag{6}$$

The boundary conditions for Eq. (5) are $\phi(y=0) = \zeta_1$ for the bottom wall and $\phi(y=h) = \zeta_2$ for the upper wall.

Eq. (5) can be non-dimensionalized as

$$\frac{\mathrm{d}^2\phi^*}{\mathrm{d}y^{*2}} = K^2\phi^* \tag{7}$$

where $\phi^* = z_0 e\phi/(k_b T)$, $y^* = y/h$, $K = \kappa h$ is the electrokinetic separation distance based on the plate height.

The electrokinetic separation distance based on the half plate height can be defined as $K_{\mathrm{esd}} = K/2$.

The boundary conditions for Eq. (7) in a non-dimensional form can be written as $\phi^*(y^* = 0) = \zeta_1^*$, where $\zeta_1^* = z_0 e\zeta_1/(k_b T)$ for the bottom wall, and $\phi^*(y^* = 1) = \zeta_2^*$, where $\zeta_2^* = z_0 e\zeta_2/(k_b T)$ for the upper wall. Its analytical solution can be written as

$$\phi* = \frac{\zeta_2^*\sinh(Ky^*) - \zeta_1^*\sinh(Ky^* - K)}{\sinh(K)} \tag{8}$$

The net charge density in a non-dimensional form is expressed as

$$\rho_e^* = \frac{\rho_e}{n_\infty z_0 e} \tag{9}$$

Taking into account Eqs. (6) and (8), Eq. (9) is found:

$$\rho_e^* = 2\frac{\zeta_1^*\sinh(Ky^* - K) - \zeta_2^*\sinh(Ky^*)}{\sinh(K)} \tag{10}$$

2.2. Hydrodynamic field

For a one-dimensional steady fully developed laminar liquid flow through a microchannel between two parallel plates, as shown in Fig. 1, the modified Navier–Stokes equation in x-direction is given by

$$0 = -\frac{\partial p}{\partial x} + \mu\frac{\partial^2 u}{\partial y^2} + E_x\rho_e \tag{11}$$

where E_x is the electric field. Pressure and flow velocity depend only on x and y, respectively.

When assuming that the pressure gradient in x-direction is constant, we can express Eq. (11) as

$$0 = \frac{P_x}{\mu} + \frac{\mathrm{d}^2 u_1}{\mathrm{d}y^2} - \frac{\varepsilon\varepsilon_0\kappa^2 E_x}{\mu}\phi \tag{12}$$

where $P_x = -\frac{\mathrm{d}p}{\mathrm{d}x}$.

Eq. (12) is a second-order differential equation; thus two boundary conditions are required to solve it. The slip boundary conditions can be expressed as $u(0) = u_{s1}$ and $u(1) = u_{s2}$, where $u_{s1} = \beta\frac{\partial u}{\partial y}|_{y=0}$ is the slip velocity along the bottom plate, $u_{s2} = -\beta\frac{\partial u}{\partial y}|_{y=h}$ is the slip velocity along the upper plate and β is the slip coefficient.

In a non-dimensional form, Eq. (12) is formulated as

$$0 = C_0 + \frac{\mathrm{d}^2 u^*}{\mathrm{d}y^{*2}} - C_1\frac{\mathrm{d}^2\phi^*}{\mathrm{d}y^{*2}} \tag{13}$$

where $u^* = u/u_0$, $C_0 = h^2 P_x/(\mu u_0)$, $C_1 = u_h/u_0$, and $u_h = E_x\varepsilon\varepsilon_0 K_b T/(z_0 e\mu)$ is the Helmholtz–Smoluchowski electroosmotic velocity. The dimensionless pressure difference can be defined as $\Delta p^* = C_0$.

Integrating Eq. (13) twice yields

$$u^* = -\frac{C_0}{2}y^{*2} + a_1 y^* + C_1\phi^* + a_2 \tag{14}$$

The constants of integration, a_1 and a_2, can be determined using the slip boundary conditions in a non-dimensional form. These can be formulated as $u^*(0) = u_{s1}^*$ and $u^*(1) = u_{s2}^*$, where $u_{s1}^* = \beta^*\frac{\partial u^*}{\partial y^*}|_{y^*=0}$ is the dimensionless slip velocity along the bottom plate, $u_{s2}^* = -\beta^*\frac{\partial u^*}{\partial y^*}|_{y^*=1}$ is the dimensionless slip velocity along the upper plate and $\beta^* = \beta/h$ is the dimensionless slip coefficient.

Applying these dimensionless slip boundary conditions, a system of two linear Eqs. (15) and (16) in two unknowns (a_1 and a_2) was found:

$$-\beta^* a_1 + a_2 = C_3 \tag{15}$$

$$(1+\beta^*)a_1 + a_2 = C_4 \tag{16}$$

where

$$C_3 = C_1\left(\left(-1-\beta^* K\,\coth(K)\right)\zeta_1^* + \frac{\beta^* K \zeta_2^*}{\sinh(K)}\right) \tag{17}$$

$$C_4 = C_0\left(\frac{1}{2}+\beta^*\right) + C_1\left(\frac{\beta^* K \zeta_1^*}{\sinh(K)} + \left(-1-\beta^* K\,\coth(K)\right)\zeta_2^*\right) \tag{18}$$

Solving this system of two linear equations yields

$$a_1 = \frac{-C_3 + C_4}{1+2\beta^*} \tag{19}$$

$$a_2 = \frac{(1+\beta^*)C_3 + \beta^* C_4}{1+2\beta^*} \tag{20}$$

The volumetric flow rate in the non-dimensional form is obtained integrating the dimensionless velocity distribution over the dimensionless cross-sectional area,

$$Q^* = \int_0^1 u^*\,\mathrm{d}y^* = \frac{J_1}{J_2} \tag{21}$$

where

$$J_1 = \frac{1}{6}\big(-6C_1\zeta_1^*\exp(K) + 3C_1\zeta_2^*\exp(K)^2 + 3a_1\sinh(K)K\exp(K) - C_0\sinh(K)K\exp(K) + 6a_2\sinh(K)K\exp(K) + 3C_1\zeta_2^* - 6C_1\zeta_2^*\exp(K) + 3C_1\zeta_1^*\exp(K)^2 + 3C_1\zeta_1^*\big) \tag{22}$$

and

$$J_2 = K\exp(K)\sinh(K) \tag{23}$$

2.3. Temperature distribution

The energy equation for a steady fully developed laminar liquid flow is given by

$$\rho c_p u\frac{\partial T}{\partial x} = k\frac{\partial^2 T}{\partial y^2} + E_x^2\sigma \tag{24}$$

where c_p, k and σ represent the specific heat, the thermal conductivity of the liquid and the electric conductivity, respectively. T is the local temperature.

The boundary conditions for Eq. (24) are expressed as $-k\frac{\partial T}{\partial y} = q_1$ for $y = 0$ and $k\frac{\partial T}{\partial y} = q_2$ for $y = h$.

The wall temperatures are defined as T_{w1} and T_{w2} for the bottom and upper wall, respectively.

For an imposed constant heat flux boundary condition, the thermally fully developed condition of

Eq. (24) gives $\frac{\partial T}{\partial x} = \frac{\mathrm{d}T_m}{\mathrm{d}x} = \text{constant}$ and $\frac{\partial^2 T}{\partial x^2} = 0$, where T_m is the bulk mean temperature, which is defined as

$$T_m = \frac{1}{A_c u_m}\int_{A_c} uT\,\mathrm{d}A_c \tag{25}$$

Also, the energy balance on a liquid in a microchannel can be expressed as

$$\rho u_m c_p\frac{\mathrm{d}T_m}{\mathrm{d}x} = \frac{q_1+q_2}{h} + E_x^2\sigma \tag{26}$$

Substituting Eq. (26) into Eq. (24), Eq. (27) is found:

$$\rho c_p u\left(\frac{1}{\rho u_m c_p}\left(\frac{q_1+q_2}{h} + E_x^2\sigma\right)\right) = k\frac{\partial^2 T}{\partial y^2} + E_x^2\sigma \tag{27}$$

Defining the dimensionless temperature as

$$T^* = \frac{T - T_m}{\frac{hq_1}{k}} \tag{28}$$

The dimensionless form of Eq. (27) can be expressed as

$$\frac{\partial^2 T^*}{\partial y^{*2}} = H_1 u^* - q_v^* \tag{29}$$

where $H_1 = \frac{1}{u_m^*}((1+\gamma)+q_v^*)$, $u_m^* = \frac{u_m}{u_0}$, $q_v^* = E_x^2\sigma\frac{h}{q_1}$ and $\gamma = \frac{q_2}{q_1}$ is the heat flux ratio.

The dimensionless boundary conditions are given by $\frac{\partial T^*}{\partial y^*} = -1$ for $y^* = 0$ and $\frac{\partial T^*}{\partial y^*} = \gamma$ for $y^* = 1$. For the dimensionless wall temperatures, they are defined as T_{w1}^* for $y^* = 0$ and T_{w2}^* for $y^* = 1$.

Integrating Eq. (29) twice and taking into account the boundary conditions, the difference between the bottom wall temperature and the local temperature can be written as

$$T_{w1}^* - T^* = -F_{b1} + F_{b2}F_{b3} - F_{b4} \tag{30}$$

where

$$F_{b1} = -\frac{1}{2}\frac{H_1}{\sinh(k)}\left(\frac{C_0}{12}y^{*4}\sinh(K) - \frac{a_1}{3}y^{*3}\sinh(K) - 2\frac{C_1\zeta_2^*}{K^2}\sinh(KY^*) + 2\frac{C_1\zeta_1^*}{K^2}\sinh(Ky^* - K) - a_2\sinh(K)y^{*2}\right) - \frac{1}{2}q_v^* y^{*2} \tag{31}$$

$$F_{b2} = H_1 C_1\big(2\zeta_2^*\big(\cosh(K)+\sinh(K)\big) - \zeta_1^*\big(\cosh(2K)+\sinh(2K)+1\big)\big) + K\big(\cosh(2K)+\sinh(2K)-1\big), \tag{32}$$

$$F_{b3} = \frac{y^*}{K(\sinh(2K) - 1 + \cosh(2K))} \tag{33}$$

$$F_{b4} = -\frac{H_1 C_1\zeta_1^*}{K^2} \tag{34}$$

The difference between the upper wall temperature and the local temperature can be expressed as

$$T_{w2}^* - T^* = -F_{u2} - F_{u1}F_{u3} - F_{u4}F_{u5} \tag{35}$$

where

$$F_{u1} = \frac{y^*}{6K(\sinh(2K) - 1 + \cosh(2K))} \tag{36}$$

$$F_{u2} = -\frac{1}{2}\frac{H_1}{\sinh(K)}\left(\frac{C_0}{12}y^{*4}\sinh(K) - \frac{a_1 y^{*3}}{3}\sinh(K) - \frac{2C_1\zeta_2^*}{K^2}\sinh(Ky^*) + \frac{2C_1\zeta_1^*}{K^2}\sinh(Ky^* - K) - a_2\sinh(K)y^{*2}\right) - \frac{q_v^*}{2}y^{*2} \tag{37}$$

$$F_{u3} = 12H_1C_1\zeta_1^*\big(\cosh(K)+\sinh(K)\big) + 6q_v^*K\big(\cosh(2K) + \sinh(2K) - 1\big) - 3H_1a_1\big(K\sinh(2K)+K - \cosh(2\mathrm{K})\big) + H_1C_0K\big(\sinh(2K)+K\cosh(2K)-1\big) - 6H_1a_2K\big(\sinh(2K)-\cosh(2K)+1\big) - 6\mathrm{H}_1C_1\zeta_2^*\big(1-\cosh(2K)\big) - 6H_1q_1\zeta_2^*\sinh(2K) - 6\gamma\mathrm{K} + 6\gamma K\cosh(2K) + 6\gamma K\sinh(2K) \quad (38)$$

$$F_{u4} = -24H_1C_1\big(\zeta_2^*\big(1+K\cosh(2K)\big) + 2K\zeta_1^*\cosh(K)\big) - 12\mathrm{K}^2q_v^*\big(1+\sinh(2K)\big) + 24\gamma K^2\cosh(2K) + 24\gamma K^2\sinh(2K) - 12H_1a_2K^2\big(\sinh(2K) + \cosh(2K)-1\big) - 8H_1a_1K^2\big(\sinh(2K) + \cosh(2K)-1\big) + 12\mathrm{K}^2\cosh(2K) + 24H_1C_1\zeta_2^*\big(\cosh(2K)+\sinh(2K)(1-K)-K\big) + 48KH_1C_1\zeta_1^*\sinh(K) + 3H_1C_0K^2\big(\sinh(2K) + \cosh(2K)-1\big) - 24\gamma K^2 \quad (39)$$

$$F_{u5} = -\frac{1}{24K^2(\sinh(2K)-1+\cosh(2K))} \quad (40)$$

The fully-developed Nusselt number may be expressed for the bottom plate wall as

$$Nu_1 = \frac{q_1h}{k(T_{w1}-T_m)} = \frac{1}{T_{w1}^*-T_m^*} \quad (41)$$

where

$$T_{w1}^*-T_m^* = \frac{1}{u_m^*}\int_0^1 u^*(T_{w1}-T)\,\mathrm{d}y^* \quad (42)$$

For the upper plate wall, it can be given by

$$Nu_2 = \frac{q_2h}{k(T_{w2}-T_m)} = \frac{\gamma}{T_{w2}^*-T_m^*} \quad (43)$$

where

$$T_{w2}^*-T_m^* = \frac{1}{u_m^*}\int_0^1 u^*(T_{w2}-T)\,\mathrm{d}y^* \quad (44)$$

The integrals $\int_0^1 u^*(T_{w1}-T)\,\mathrm{d}y^*$ in Eq. (42) and $\int_0^1 u^*(T_{w2}-T)\,\mathrm{d}y^*$ in Eq. (44) are solved numerically using the trapezoidal rule.

3. Results and discussion

To investigate and analyze the effects of the slip coefficient, the pressure difference and the heat flux on the liquid flow and the thermal characteristics in a microchannel between two plates, a computer program was written using the equations found in Section 2. The following constant data were used for the simulations accomplished: $n_\infty = 6.022\times10^{20}\ \mathrm{m}^{-3}$, $\varepsilon_0 = 8.854\times10^{-12}\ \mathrm{C\,m^{-1}\,V^{-1}}$, $\varepsilon = 80$, $z_0 = 1$, $K_{\mathrm{esd}} = 40.71$, $E_x = 5\times10^4\ \mathrm{V\,m^{-1}}$, $\mu = 0.001\ \mathrm{kg\,m^{-1}\,s^{-1}}$, $\sigma = 0.001\ \Omega^{-1}\,\mathrm{m}^{-1}$, $L = 0.01$ m, $h = 25\times10^{-6}$ m, $q_1 = 1200\ \mathrm{W\,m^{-2}}$, $\Delta p = 30$ kPa, and $u_0 = 1\ \mathrm{m\,s^{-1}}$.

3.1. Effect of the slip coefficient on the flow velocity

To examine the effect of the dimensionless slip coefficient on dimensionless flow velocity, the dimensionless pressure difference and the heat flux ratio were kept constant with values of 1.9 and 1, respectively. The dimensionless slip coefficients of 0, 0.05 and 0.1 were selected. Fig. 2 represents flow velocity distribution in the microchannel cross-section. The curve with the dimensionless slip coefficient of 0 corresponds to the known fluid velocity profile with no slip effect. The other curves represent the fluid velocity profile with slip effect. There, it can be seen clearly that the increase in the dimensionless slip coefficient leads to higher dimensionless flow velocity. The curve in the dimensionless volumetric flow rate as a function of the dimensionless slip coefficient shown in Fig. 3, indicates that the dimensionless volumetric flow rate augments with increasing

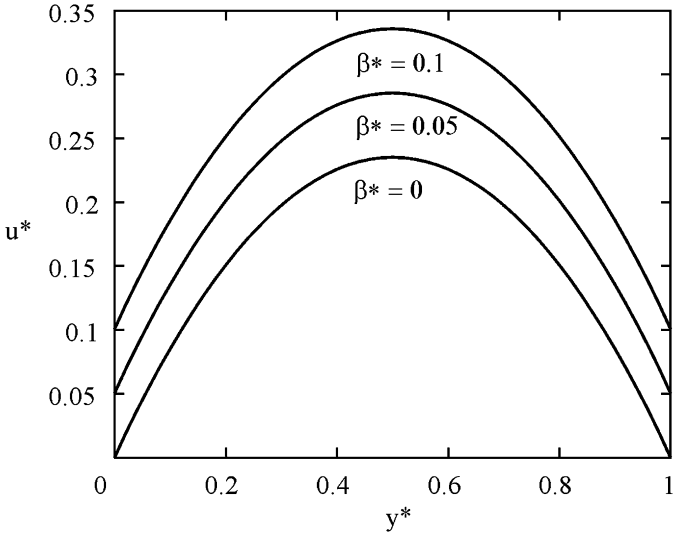

Fig. 2. Dimensionless flow velocity versus dimensionless distance between the plates (parameter: dimensionless slip coefficient).

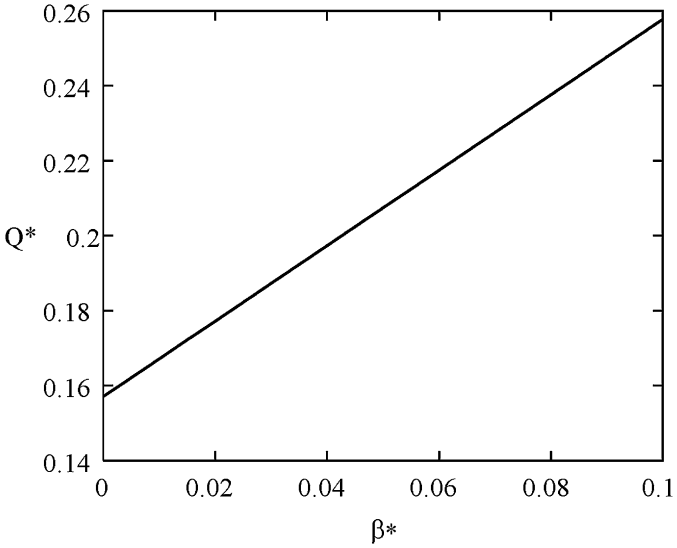

Fig. 3. Dimensionless volumetric flow rate versus dimensionless slip coefficient.

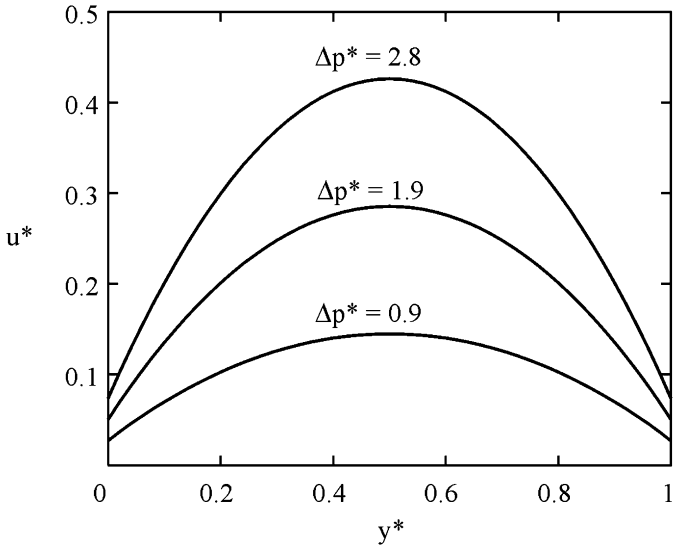

Fig. 4. Dimensionless flow velocity versus dimensionless distance between the plates (parameter: dimensionless pressure difference).

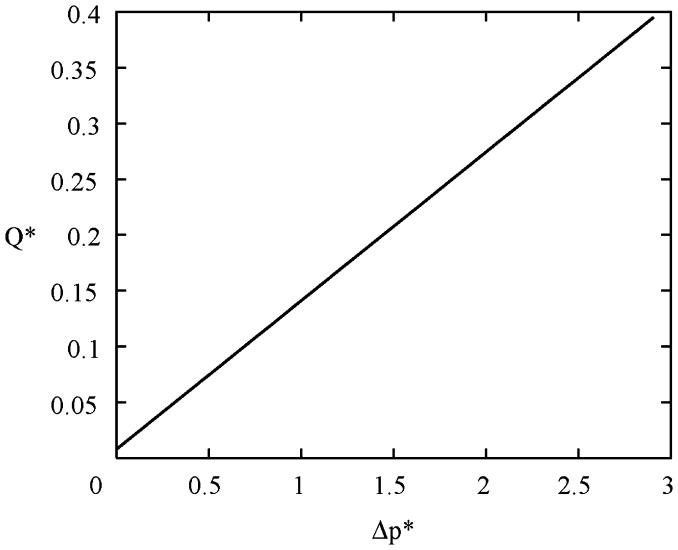

Fig. 5. Dimensionless volumetric flow rate versus dimensionless pressure difference between microchannel inlet and outlet.

dimensionless slip coefficient. Indeed, the EDL causes a large reduction in volumetric flow rate, whereas, liquid slip counteracts the effect by the EDL and induces a larger volumetric flow rate. The comparison of the dimensionless volumetric flow rates with $\beta^* = 0$ and $\beta = 0.1$ yields an augmentation of 64.1% in dimensionless volumetric flow rate.

3.2. Effect of the pressure difference on the flow velocity

To investigate the effect of the dimensionless pressure difference on the dimensionless flow velocity, the dimensionless slip coefficient and the heat flux ratio were kept constant with values of 0.05 and 1, respectively. The dimensionless pressure differences of 0.9, 1.9, 2.8 were selected. Fig. 4 shows the variation of the flow velocity as a function of the distance between the plates for three pressure differences. There, it is noted that flow velocity increases when the pressure difference between the microchannel inlet and outlet increases. The reason for this is that increasing dimensionless pressure difference between the microchannel inlet and outlet induces a larger dimensionless volumetric flow for a fixed microchannel cross-section as showed in Fig. 5, thus this leads to higher velocity. In comparison the dimensionless volumetric flow rates obtained for a pure electro-osmotic flow, $\Delta p^* = 0$, with that corresponding with $\Delta p^* = 2.8$, a ratio of 49.4 was found between both volumetric flow rates.

3.3. Effect of the slip coefficient on the wall temperature–local temperature difference

To predict the effect of the dimensionless slip coefficient on the dimensionless wall temperature–local temperature difference, the dimensionless pressure difference and the heat flux ratio were kept constant with the values of 1.9 and 1, respectively. The dimensionless slip coefficients of 0 and 0.1 were selected. Fig. 6 shows the variation of the dimensionless difference between the wall temperature and the local temperature

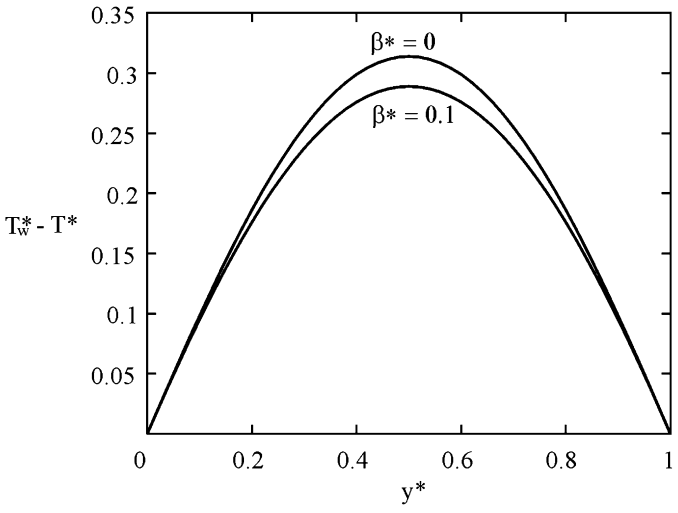

Fig. 6. Dimensionless wall temperature–local temperature difference versus dimensionless distance between the plates (parameter: dimensionless slip coefficient).

as a function of the dimensionless distance between the plates for two different slip coefficients. From this figure, it can be observed that the dimensionless slip coefficient has an influence on the maximum value of the dimensionless difference between wall temperature and local temperature. This dimensionless difference decreases with increasing dimensionless slip coefficient, i.e., the effect of the liquid slip tends to increase the flow velocity and hence the convection heat transfer. This affects the temperature distribution in the microchannel.

3.4. Effect of the heat flux on the wall temperature–local temperature difference

Three different combinations of the heat flux ratio, 0, 0.5 and 1, were considered to analyze it effect on the dimensionless wall temperature–local temperature difference, as shown in Fig. 7. The dimensionless slip and the dimensionless pressure

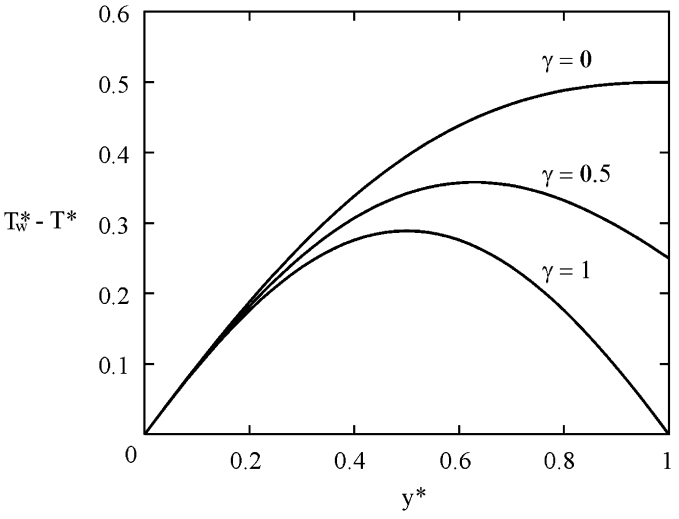

Fig. 7. Dimensionless wall temperature–local temperature difference versus dimensionless distance between the plates (parameter: heat flux).

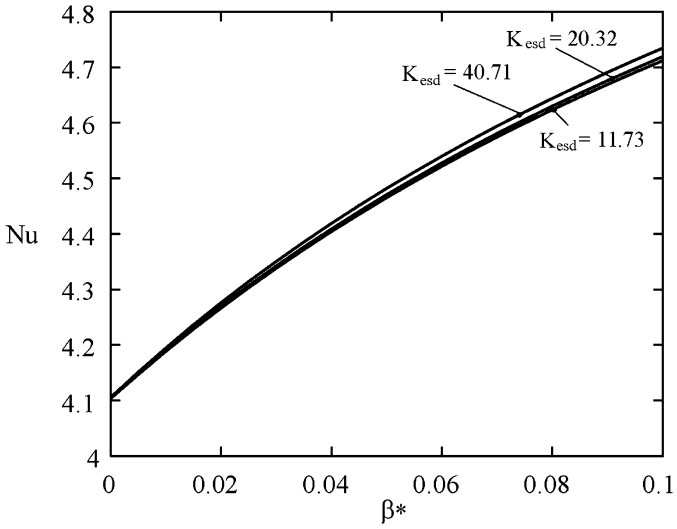

Fig. 8. Nusselt number versus dimensionless slip coefficient.

difference of 0.05 and 1.9 were kept constant. In Fig. 7, it can be seen that for a heat flux ratio of 1, the dimensionless difference between wall temperature and local temperature is symmetric. A decrease in the value of the heat flux ratio increases the asymmetry in the distribution of temperature. The heat flux ratio of 0 corresponds to a special case of asymmetry boundary condition with a heating bottom wall and a adiabatic upper wall. This heat flux boundary condition strongly affects the dimensionless wall temperature–local temperature difference on the upper wall.

3.5. Effect of the slip coefficient on the Nusselt number

Fig. 8 shows the effect of the dimensionless slip coefficient on the Nusselt number for the heat flux ratio of 1 and the dimensionless pressure difference of 1.9. From this figure, it can be observed that the Nusselt number increases when the dimensionless slip coefficient increases. This is due to the liquid slip in the wall-liquid interface which leads to higher velocity and hence to greater convection heat transfer. In the no-slip case, the Nusselt number at the upper and bottom walls is 4.1 as depicted in Fig. 8. Also, The effect of the electrokinetic separation distance on the Nusselt number was examined. It was observed from Fig. 8 that the Nusselt number increases with decreasing electrokinetic separation distance. This is because, for a higher electrokinetic separation distance, the influence of the EDL is predominant only at the zone near the microchannel wall. For small electrokinetic separation distance, the EDL has a significant effect on the liquid flow: the EDL at the wall–liquid interface induces a large reduction of liquid flow velocity, that affects the convection heat transfer with decreasing electrokinetic separation distance.

3.6. Model verification

In order to compare the developed model with the results obtained using the analytical approach, described in [4], for the electrokinetic flow and heat transfer in a microchannel between two plates, the developed model was transformed to achieve the same boundary conditions as in [4]. Fig. 9 represents the variation of the difference between the wall temperature and the local temperature as a function of the plate height for $\Delta p^* = 1.87$, $\beta^* = 0$, $\gamma = 0.75$ and $K_{esd} = 40.71$. It can be seen that there is good harmony between the results of the analytical approach described in [4] and those from the present work.

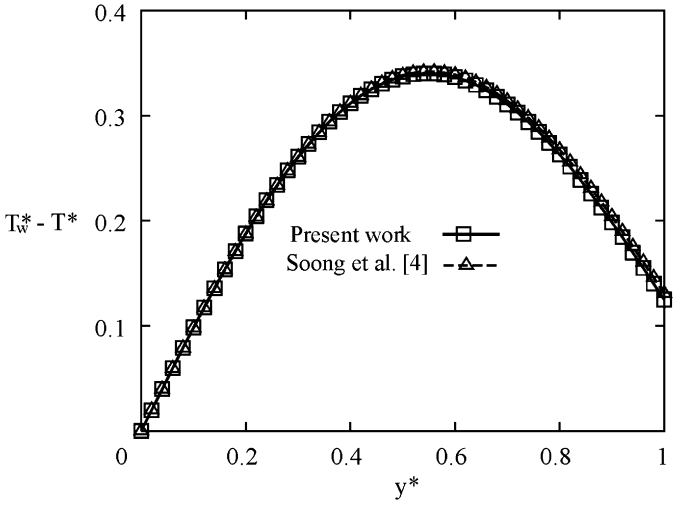

Fig. 9. Comparison of the dimensionless wall temperature–local temperature difference between the present work and the study of Soong et al. [4].

4. Conclusion

In this paper, a mathematical model of the liquid flow in a microchannel between two parallel plates was developed and analyzed, taking into consideration the slip velocity and the heat flux on the plate walls. Based on the Poisson–Boltzmann, the modified Navier–Stokes and the energy equations, the expressions of the electric potential, the flow velocity, the volumetric flow rate, the difference between the wall temperature and local temperature, and the mean Nusselt number were found accounting for the combined effect of the pressure gradient and electro-osmosis. The results obtained show that the variation of

the slip coefficient, the pressure difference, the heat flux and the electrokinetic separation distance affect the thermal and the liquid flow behavior in a microchannel significantly but in different ways. The comparison of the developed model with the results obtained using an analytical approach described in [4] shows good harmony.

Acknowledgements

The authors are grateful to Institutional Fund of Research of the University of Quebec (FIR).

References

[1] G.S. Kandlikar, S. Garimella, D. Li, S. Colin, M.R. King, Heat Transfer And Fluid Flow in Minichannels, Elsevier, Oxford, UK, 2006.
[2] N.-T. Nguyen, S.T. Wereley, Fundamentals and Applications of Microfluidics, Artech House Publishers, Boston, London, 2002.
[3] D.C. Tretheway, C.D. Meinharta, Apparent fluid slip at hydrophobic microchannel walls, Physics of Fluids 14 (3) (2002) L9–L12.
[4] C.Y. Soong, S.H. Wang, Theoretical analysis of electrokinetic flow and heat transfer in a microchannel under asymmetric boundary conditions, Journal of Colloid and Interface Science 265 (2003) 202–213.
[5] C.Y. Soong, S.H. Wang, P.Y. Tzeng, Analysis of fully-developed forced convection of electrokinetic flow in flat microchannels at prescribed wall temperatures or wall heat fluxes, Transactions of the Aeronautical and Astronautical Society of the Republic of China 36 (1) (2004) 29–44.
[6] Z. Guo, T.S. Zhao, Y. Shi, Lattice Boltzmann algorithm for electro-osmotic flows in microfluidic devices, Journal of Chemical Physics 122 (2005), 144907, pp. 1–10.
[7] T.S. Zhao, Q. Liao, Thermal effects on electro-osmotic pumping of liquids in microchannels, Journal of Micromechanics and Microengineering 12 (2002) 962–970.
[8] K. Horiuchi, P. Dutta, A. Hossain, Joule heating effects in mixed electroosmotic and pressure driven microflows under constant wall heat flux, Journal of Engineering Mathematics 54 (2006) 159–180.
[9] K. Horiuchi, P. Dutta, Joule heating effects in electroosmotically driven microchannel flows, International Journal of Heat and Mass Transfer 47 (2004) 3085–3095.
[10] K. Horiuchi, P. Dutta, Heat transfer characteristics in mixed electroosmotic and pressure driven micro-flows, JSME International Journal Series B 49 (2006) 812–819.
[11] D. Maynes, B.W. Webb, Fully-developed thermal transport in combined pressure and electro-osmotically driven flow in microchannels, Journal of Heat Transfer 125 (5) (2003) 889–895.
[12] D. Maynes, B.W. Webb, The effect of viscous dissipation in thermally fully-developed electroosmotic heat transfer in microchannels, International Journal of Heat and Mass Transfer 47 (2004) 987–999.
[13] G. Tunc, Y. Bayazitoglu, Heat transfer in rectangular microchannels, International Journal of Heat and Mass Transfer 45 (2002) 765–773.
[14] S. Yu, T.A. Ameel, Slip-flow heat transfer in rectangular microchannels, International Journal of Heat and Mass Transfer 44 (2001) 4225–4234.
[15] S. Yu, T.A. Ameel, Slip flow convection in isoflux rectangular microchannels, Journal of Heat Transfer 124 (2) (2002) 346–355.
[16] J. Yang, D.Y. Kwok, Effect of liquid slip in electrokinetic parallel-plate microchannel flow, Journal of Colloid and Interface Science 260 (2003) 225–233.